Determination of heat of vaporization and vapor pressure by micro-liter fuel droplet vaporization

Wanjun Dang* and Shyam Menon †
Louisiana State University, Baton Rouge, LA, 70808

Fuel physical properties including vapor pressure and heat of vaporization are of great importance for spray atomization, mixing and evaporation processes in IC engines affecting their combustion and emission characteristics. This work utilizes small volumes and heated fuel droplets in the order of microliters to study the evaporation process. Measurements are obtained at atmospheric pressure over a range of temperatures relevant to in-cylinder fuel injection processes. Single droplets generated by a piezoelectric device at elevated temperatures are stroboscopically imaged to record the droplet size change during evaporation. By tracking the droplet evaporation process and modeling it using the Abramzon-Sirignano model, vapor pressure and heat of vaporization can be estimated. Measurements of these two physical properties of n-heptane and isooctane are compared with literature data at different temperatures. This novel property measurements and prediction procedure provides a pathway to identify potential fuel candidates for further development as drop-in replacements or blending components for use in advanced, high performance, low-emission engines.

I. Introduction

Fuel spray plays a key role in the overall performance and emissions of direct-injected, liquid hydrocarbon-fueled, internal combustion (IC) engines. The fuel injection process and resulting spray introduces fuel into the engine cylinder. The subsequent spray breakup, atomization, evaporation and, fuel-air mixing phenomena play a key role in the ensuing combustion process.

Fuel physical properties play a critical role in the above-mentioned in-cylinder processes. Spray breakup through atomization, and its penetration into the cylinder volume are impacted by fuel surface tension and viscosity. Once atomized into a distribution of finely-sized droplets, evaporation and fuel-air mixing processes are directly coupled to the heat of vaporization and vapor pressure of the fuel, as dictated by the ambient conditions surrounding the fuel droplets. Heat of vaporization or latent heat is the energy required for phase change of the liquid fuel. Vapor pressure is a measure of the pressure exerted by the fuel vapor in thermodynamic equilibrium condition with its liquid phase. Heat of vaporization (HOV) and vapor pressure are directly related to each other through the Clausius-Clapeyron equation,

$$ln(P/P_0) = -\Delta HOV/RT + C \tag{1}$$

where P is the vapor pressure at the corresponding temperature, T, R is the gas constant, P_0 is the reference pressure and C is the intercept of the linear fit from plotting the natural log of vapor pressure against temperature.

The impact of HOV is primarily through in-cylinder thermodynamics as affected by the fuel droplet evaporation processes leading to the formation of the fuel-air mixture. The energy required for evaporation is provided by the ambient air surrounding the droplets in the engine cylinder. In the process, as fuel evaporates, it results in cooling of the in-cylinder charge. This reduction in charge temperature, and corresponding increase in intake air density results in improved volumetric efficiency of gasoline engines, particularly at part load conditions [1]. Evaporative cooling as affected by fuel HOV also has a significant effect on knock suppression in direct-injected (DI) gasoline engines. Previous studies conducted on downsized, turbo-boosted engines have shown that evaporative cooling provides an effect comparable to increasing the octane rating of the fuel by about 5 units, allowing an increase in compression ratio by about 1 unit [2]. Knock resistance of a fuel is commonly expressed through the octane index (OI) [3], expressed as,

$$OI = RON - K * S \tag{2}$$

---

*Graduate Research Assistant, Mechanical and Industrial Engineering Department, wdang3@lsu.edu.
†Assistant Professor, Mechanical and Industrial Engineering Department, smenon@lsu.edu.

where RON is the Research Octane Number and S is the octane sensitivity ($RON - MON$). K is an engine constant that depends on pressure-temperature history of the unburned charge in the engine cylinder and typically has negative values at the most knock-limited operating conditions. While K is not a fuel property, the end-gas pressure-temperature history which K relates to, is affected by fuel composition and properties including HOV. Higher HOV reduces charge temperature, leading to more negative values of K, and thus improves fuel anti-knock properties. This is directly evidenced by numerous studies considering the impact of ethanol and other alcohol blends on engine knock [2, 4, 5].

Vapor pressure is another important physicochemical property, widely used in assessing the quality of gasoline along with other quantities such as distillation parameters, specific gravity, octane number and octane index. Vapor pressure is directly related to the volatility of the fuel and has a direct influence on engine performance as well as fuel production and transportation logistics. Fuel vapor pressure is required to meet specific standards to ensure safety considerations in the transport and storage of fuels to avoid accidents and minimize losses through evaporation. Fuels with lower vapor pressure are harder to vaporize resulting in poor combustion efficiency [6]. On the other hand, fuels with high vapor pressure can generate volatile organic compounds leading to uncontrolled air-fuel ratio affecting the combustion process. These considerations have made it a requirement to maintain fuel vapor pressure within an acceptable range.

Given their significant influence on fuel transportation, storage, and evaporation and combustion characteristics impacting engine performance, standard testing approaches have been established for measuring HOV and vapor pressure. Classical methods for measuring HOV for fuel blends have utilized the Clausius-Clapeyron equation but with limited success [7]. More recently, a Differential Scanning Calorimetry (DSC)/Thermogravimetric Analysis (TGA) approach has been used to measure total HOV of gasoline-ethanol blends [7]. Gasoline volatility is typically expressed through the Reid Vapor Pressure (RVP). RVP can be measured through a variety of Reid methods (ASTM D-323, D-4953, and D-5191) [8, 9].

While standard techniques of HOV and vapor pressure measurement can successfully evaluate fuel properties for pure components and fuel blends, this study is motivated by a desire to develop screening approaches that can utilize small quantities of liquid fuels and rapidly evaluate their physical properties. Specifically it is desired to work with fuel quantities on the order of 20 μL and produce results within seconds. This will enable rapid screening approaches to downselect from a large number of candidate fuels that can be narrowed down to a fewer number based on threshold requirements for physical properties such as viscosity, surface tension, HOV, and vapor pressure. Development of rapid screening tools is the objective of ongoing work through the DOE's (Department of Energy) Co-Optima initiative. This initiative aims to identify potential gasoline blendstocks with viable biomass-derived production pathways to incorporate renewable domestic biomass into the gasoline supply chain [10]. Previous work by the authors focused on small-volume, high-throughput approaches for surface tension and viscosity measurement [11]. This work will pursue similar objectives with respect to determining HOV and vapor pressure for liquid fuels.

The paper is laid out as follows. The approach used in this work that leverages droplet evaporation processes as modeled by a zero-dimensional transient simulation that captures droplet size change for stationary and moving liquid fuel droplets is discussed. The experimental setup and procedure used to measure fuel droplet evaporation rate at controlled temperature conditions is presented and discussed. Next, results are presented for HOV and vapor pressure calculations for stationary and moving droplets based on simulated droplet evaporation rates. Following this, HOV and vapor pressure calculation results are presented for moving droplets as obtained using experimental data. Results are discussed and finally conclusions are presented.

II. Approach

As described in the introduction, this work is motivated by development of techniques for HOV and vapor pressure measurement of liquid hydrocarbon fuels, suitable for use in high-throughput, rapid-screening approaches for bio-derived gasoline blendstocks. Ideally the measurement technique for HOV and vapor pressure can be integrated with a droplet-oscillation based approach developed for fuel viscosity and surface tension measurement [11]. These considerations have motivated the pursuit of a droplet-evaporation based approach to measure HOV and vapor pressure. This approach offers the following advantages:

- Seamless integration with droplet-oscillation based surface tension and viscosity measurements.
- Use of micron-sized droplets ensures measurements require small sample sizes ($O(\mu L)$).
- Size changes evaluated for moving, evaporating droplets as needed for HOV and vapor pressure measurement can be

achieved rapidly ($O(s)$).

- Physical property evaluation techniques based on droplet oscillation and evaporation can be easily integrated with chemical kinetic property evaluation techniques being developed using a micro-combustor setup [12].

A liquid fuel droplet subjected to a controlled temperature environment undergoes evaporation under stationary or moving conditions. The evaporation process for small droplets involving heat and mass transfer is controlled primarily by the ambient conditions and liquid properties including HOV and to a smaller degree by second-order effects such as circulation within the droplet, gas motion around the stationary or moving droplet, and water condensation on the droplet surface. A large body of work has been carried out to model droplet evaporation processes under various conditions (stationary/moving/oscillating) incorporating various levels of complexity. A number of reviews of droplet modeling approaches can be found in literature [13, 14]. The approach used in this work is to use an appropriate droplet evaporation model to calculate HOV and vapor pressure, using as input data, the droplet size change as a function of time as measured by an experimental setup. In developing this measurement approach, at first the input data for droplet size change was generated using simulations, following which, data obtained from an experimental setup was used to determine HOV and vapor pressure. Vapor pressure and HOV are coupled to each other through the Clausius-Clapeyron equation presented earlier in Eq. 2.

The proposed approach is similar to that followed by Ray [15] who used observations of size change of evaporating droplets at stationary conditions as obtained through droplet levitation to estimate ultra-low vapor pressures of fluids used in aerosol research. Ray used a Maximum Likelihood Estimation (MLE) approach to determine fluid physical properties including HOV and vapor pressure as well as molecular dynamic parameters such as the parameters relating to the Lennard-Jones potential. This approach differs from Ray's work in that the focus is on using moving droplets to allow a simpler experimental setup without the need to levitate droplets in a constant temperature chamber. The MLE approach followed by Ray was motivated by the desire to use multiple experimental datasets for droplet evaporation obtained at different constant temperatures and ambient gas compositions. Having a higher number of experimental datasets than the number of unknowns resulted in an over-constrained set of equations. The MLE approach was then used to solve this set of equations to obtain the best estimation for the unknown variables that would minimize global error in the solution set. The approach allows minimizaztion of random error introduced by the experimental measurements on the solution set.

In the current work also, it is desired to minimize random error introduced by experimental data sets for droplet evaporation. To this end the overall approach followed is described by the following steps:

1. Obtain droplet size change as a function of time for the desired fuel using an experimental or computational approach at the desired ambient temperature and pressure conditions.
    - Droplet size change for a stationary droplet is obtained using a simple d^2 model.
    - Droplet size change for a moving droplet is obtained using the Abramzon-Sirignano (AS) model computationally and using a droplet generator based approach experimentally.
2. Use droplet size change data to calculate evaporation slope
3. Repeat the above steps with different ambient gas compositions to determine a set of different evaporation slopes.
4. Use the droplet evaporation model (AS model) in reverse with evaporation slope as the input and use a non-linear least squares approach to calculate HOV and vapor pressure that minimizes errors across the multiple data sets obtained with different ambient gas compositions.

The use of different ambient gas compositions allows multiple simulation datasets to be established to pursue the use of non-linear least squares to minimize error in HOV and vapor pressure estimation. In the case of experiments, multiple data sets would be acquired using the same ambient gas (air), and again, the non-linear least squares approach would be used to reduce effects of random error arising from the measurements.

The Abramzon and Sirignano model [14], which builds upon the classical droplet evaporation model is used to simulate the evaporation of a single liquid fuel droplet in order to obtain the droplet size change. To consider the effect of convective heat and mass transfer, the "film theory" introduces a vapor-gas film between the droplet surface and ambient gas flow, providing resistance to heat and mass exchange, as represented schematically in Figure 1. The model makes the following assumptions:

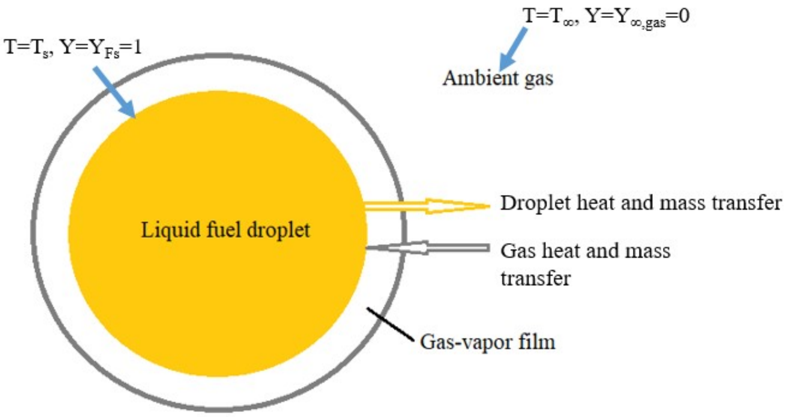

Fig. 1 Schematic of "film theory" in droplet

- A quasi-steady approximation is made for the gas phase heat and mass transfer.
- The droplet has a single downward velocity component while the ambient gas is stationary.
- Thermo-physical properties are functions of temperatures only.
- The distribution of temperature and fuel vapor concentration along the droplet surface is assumed to be uniform.
- An 'infinite conductivity model' is considered which assumes a spatially uniform but time-varying temperature distribution within the droplet.
- The velocity field within the moving droplet is disregarded.

The model solves the following set of ordinary differential equations:

Droplet motion:

$$\frac{dx}{dt} = u \tag{3}$$

Droplet velocity change:

$$\frac{du}{dt} = 3\frac{C_D}{D_s}(\frac{\rho_\infty}{\rho_L})|u_\infty - u|(u_\infty - u) + g \tag{4}$$

Droplet diameter change:

$$\frac{dD_s}{dt} = -\frac{2\dot{m}}{\pi \rho_L D_s^2} \tag{5}$$

Droplet temperature change:

$$\frac{dT_s}{dt} = \frac{Q_L + HOV \bullet \dot{m}}{m_L C_{pl}} \tag{6}$$

where T_s is the surface temperature of the droplet, Q_L is the heat penetrating into the liquid phase.

The Nusselt and Sherwood numbers are,

$$Nu_0 = 2 + 0.552 Re^{1/2} Pr^{1/3} \tag{7}$$

$$Sh_0 = 2 + 0.552 Re^{1/2} Sc^{1/3} \tag{8}$$

The Spalding mass transfer number is calculated as,

$$B_M = \frac{Y_{FS} - Y_{F,air}}{1 - Y_{FS}} \tag{9}$$

where Y_{FS} is mass fuel vapor fractions at the droplet surface.

The Spalding heat transfer number is,

$$B_T = \frac{\bar{C}_{PF}(T_\infty - T_s)}{L(T_s) + Q_L/\dot{m}} \tag{10}$$

And the corrected value of the Spalding heat transfer number is,

$$B_T = (1 + B_M)^\phi - 1 \tag{11}$$

where

$$\phi = \frac{\bar{C}_{pF}}{\bar{C}_{pg}} \frac{Sh^*}{Nu^*} \frac{1}{Le} \tag{12}$$

The film correction factors for the film thickness are calculated as,

$$F_M = (1 + B_M)^{0.7} \frac{ln(1 + B_M)}{B_M} \tag{13}$$

$$F_T = (1 + B_T)^{0.7} \frac{ln(1 + B_T)}{B_T} \tag{14}$$

The modified Sherwood number for an evaporating droplet is calculated using,

$$Sh^* = 2 + \frac{(Sh_0 - 2)}{F_M} \tag{15}$$

The modified Nusselt number is,

$$Nu^* = 2 + \frac{(Nu_0 - 2)}{F_T} \tag{16}$$

The instantaneous droplet vaporization rate is calculated using,

$$\dot{m} = 2\pi\bar{\rho}_g\bar{D}_g r_s Sh^* ln(1 + B_M) \tag{17}$$

The set of equations above (Eq. 3–Eq. 17) can be solved to predict droplet motion, and temperature and size change as a function of time. The process can be repeated using different ambient gases in order to generate multiple data sets for the same fuel droplet. In the case of experimental data, measurements will yield droplet size as a function of time under moving, evaporating conditions. In both cases (simulation and experiment), droplet size change as a function of time can be used to estimate a droplet evaporation slope:

$$K = \frac{(D^2 - D_0)^2}{t - t_0} \tag{18}$$

The next steps illustrate the technique described by the flowchart in Figure 8 to obtain HOV and vapor pressure using droplet evaporation slope as obtained from the simulations or the experiment. Equation (19) is solved to obtain vapor pressure using as input, the mass fraction of fuel on the droplet surface evaluated using Eq. (20), which uses the slope as obtained from the simulation data or experiments. Note that Eq. (19) is solved using non-linear least squares when there are multiple droplet evaporation slopes obtained for the same fuel as obtained from the simulations (for different ambient gases) or from the experiment (as obtained from multiple experimental data sets).

$$P = \frac{Y_{FS} MW_{air}}{MW_l + Y_{FS}(MW_{air} - MW_l};} \tag{19}$$

$$Y_{FS} = 1 - \frac{1}{B_M + 1} = 1 - e^{-\frac{K\rho_l}{4\bar{\rho}_g \bar{D}_g Sh^*}} \tag{20}$$

Heat of vaporization can be solved from Clausius–Clapeyron equation as following,

$$HOV = -lnP \frac{R_u}{MW_l(\frac{1}{T} - \frac{1}{T_{boil}})}; \tag{21}$$

where R_u is universal gas constant, T_{boil} is the boiling point of the fuel.

For stagnant droplet in isothermal evaporation condition, the evaporation rate can be described as following,

$$\dot{m} = 4\pi\bar{\rho_g}\bar{D_g}r_s ln(1 + B_M) \tag{22}$$

Vapor pressure and heat of vaporization can be calculated using Eqn (19) and Eqn (21). The only difference is the calculation for B_M, which can be expressed as following,

$$B_M = e^{\frac{K\rho_l}{8\bar{\rho_g}\bar{D_g}}} - 1; \tag{23}$$

III. Experiment

A. Setup

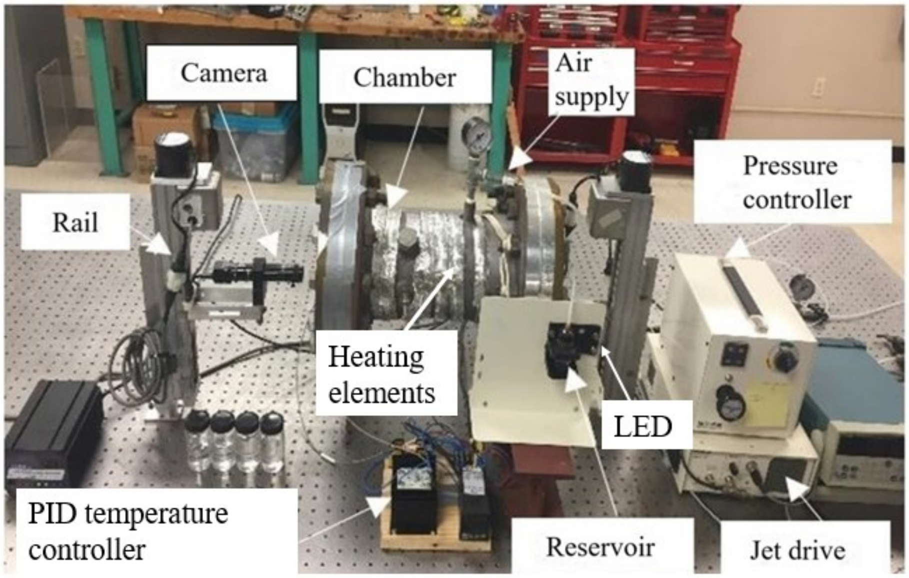

Fig. 2 Droplet generator setup for droplet size measurement

Figure 2 shows the major components of the experimental setup for droplet evaporation tests. A PID controller (Extech 48VFL) along with a heating element wrapped around the chamber are used to control the chamber temperature. The piezoelectric droplet generator(Microfab PH-47) injects a continuous stream of droplets into the chamber. Fuel is supplied to the droplet generator from a reservoir kept outside the chamber at room temperature(22°C). The temperature of the droplet at the nozzle orifice before injecting is deemed as the same temperature of chamber gas. A signal generator (Microfab JetDrive V (CT-M5-01)) provides pulses to actuate the droplet generator. The piezoelectric element on the actuator expands or contracts according to the polarity of the signal. Droplets are formed at the nozzle tip as a result of the fast deformation of the piezoelectric material. The pressure controller (MicroFab CT-PT-21) is used to select positive or negative back pressure to sustain a balancing force on the fluid column at the exit plane of the nozzle. The back pressure is provided by a compressed air source and a vacuum pump (Koge electronic, KPV20A-6A), which respectively provide positive and negative back pressures to the pressure controller. For the test cases presented in this work, droplet sizes ranged from 50-70 μm in diameter, and initial velocity leaving the nozzle is between 0.5-1 m/s. The frequency of the waveform pulse controls the droplet spacing. A machine vision camera (Sentech STC-MB33USB) mounted on a vertical traverse is used to obtain real-time images of the droplets at different locations after being injected from the nozzle. The camera has optical access into the chamber through the quartz windows located on either side of the pressure chamber. An LED strobe located at the opposite end of the chamber provides the light source for the camera. The strobed imaging approach, where the strobe signal is successively delayed from the droplet generation signal, allows for capturing droplets at different physical distances downstream from the nozzle exit plane. This approach provides a significantly easier way to track droplet evaporation rather than following a single droplet using a high-speed imaging technique.

To conduct the tests, the chamber doors are closed and the chamber is pressurized to the desired ambient pressure. In this case, all tests were conducted at atmospheric conditions. Next, the temperature controller is set to the desired set-point. Once the desired temperature is reached inside the chamber, the back pressure controller is used to purge some of the fuel thereby producing a well-defined liquid meniscus which can be seen from the camera interface to a computer. Next, using the back pressure controller, the meniscus is carefully aligned with the exit plane of the glass nozzle. Once aligned, the desired waveform pulse is applied to produce the liquid droplet train with the required frequency. The camera is used to take images of the droplets at various downstream locations from the nozzle by moving it using the vertical traverse. The distance that the camera moves along the vertical traverse is measured and used to calculate how far the droplets travelled.

B. Fuels tested

Tests were conducted using pure *n*-heptane and iso-octane at two constant temperatures of 40 and 50°C. Measurements were also obtained using various blends of *n*-heptane and iso-octane, but the discussion in this paper will be limited to the results obtained using pure components. *N*-heptane and iso-octane are chosen due to these two components being Primary Reference Fuels (PRF's), PRF's and their blends are used extensively to characterize combustion quality and knock resistance for IC engines. Iso-octane has an octane rating of 100 while *n*-heptane has an octane rating of 0. An octane rating of 100 indicates the highest propensity for knocking.

IV. Results and discussion

Simulation and experimental results for fuel droplet evaporation and subsequent prediction of HOV and vapor pressure are discussed in this section.

A. Simulation of stagnant and moving droplet evaporation

The equation set (Eq. 3–17) representing the Abramzon-Sirignano droplet evaporation model were solved using Matlab at different ambient temperatures and ambient gas compositions in order to generate data sets for use in evaluating the inverse approach to find HOV and vapor pressure. These data sets can be thought of as "training data" to validate the proposed approach to calculate HOV and vapor pressure. The initial conditions for the simulation include setting the initial droplet diameter to 60 μm and initial velocity to 1 m/s for all cases. Ambient pressure in all cases is 1 atm. The initial temperature of the droplet is assumed to be the same as that of the ambient gas. This assumption is consistent with the experimental configuration where the droplet generator is placed in the heated chamber and any transient heating of the droplet can be neglected, especially given the small droplet sizes and high initial velocity. Transport properties for the liquid fuels are obtained using Cantera and other sources [16, 17]. The average physical properties in Eqn (17) in the gas film are evaluated using the reference conditions based on a "1/3 rule" [14].

Figure 3 shows simulation results obtained for an *n*-heptane droplet undergoing evaporation in air at a constant temperature of 50 °C under stationary and moving conditions. Droplet diameter, dimensionless diameter ratio, velocity, and dimensionless evaporation rate are plotted as a function of time. From the trends of Figure 3(a), the diameter of the moving droplet is seen to decrease faster than that of the stagnant droplet. This makes intuitive sense given the contribution of convection induced mass transfer and can also be deduced from the equations. Since Sh^*>2 for the moving droplet and Sh^*=2 for the stagnant droplet as seen in Eqn (17), if the same Y_{FS} is assumed, Eqn (20) predicts that the evaporation slope for the moving moving droplet is larger than that for the stagnant droplet. As droplet velocity decreases with time and approaches 0, Sh^* is very close to 2. This causes the evaporation rate for both cases to reach the same value at around 0.035s. Within the first 0.035s, the evaporation rate of moving droplet is higher than that of the stagnant droplet. After 0.035s, the stagnant droplet has higher evaporation rate due to a smaller mass loss rate from the stagnant droplet compared to the moving droplet. Figure 3(c) shows the velocity of the moving droplet undergoes a rapid decline in the initial stages (0–10ms) followed by a much slower rate of decrease. The drag force is proportional to the square of the droplet velocity. This force has a large value initially as the droplet is ejected from the nozzle with the initial velocity. This causes the rapid decrease in initial velocity of the droplet.

Figure 4 shows evaporation simulation results for the stagnant and moving iso-octane droplet in air at three different temperatures (30, 60, and 85 °C). As temperature increases, evaporation rate also increases. At the same temperature, the moving droplet case shows a higher evaporation rate and larger diameter reduction as compared to the stagnant droplet case as seen in Fig. 3.

Figure 5 shows the droplet diameter squared for an iso-octane droplet diameter as it changes with time while evaporating in different ambient gas compositions at 30 °C. Among three ambient gases, Helium gives the steepest decrease of the droplet diameter, and CO_2 has the slowest decrease of droplet diameter.Helium has the highest diffusion coefficient among three gases, and hence results in the highest evaporation rate. On the other hand, CO_2 has the lowest diffusion coefficient among the three gases, resulting in the slowest droplet size reduction.

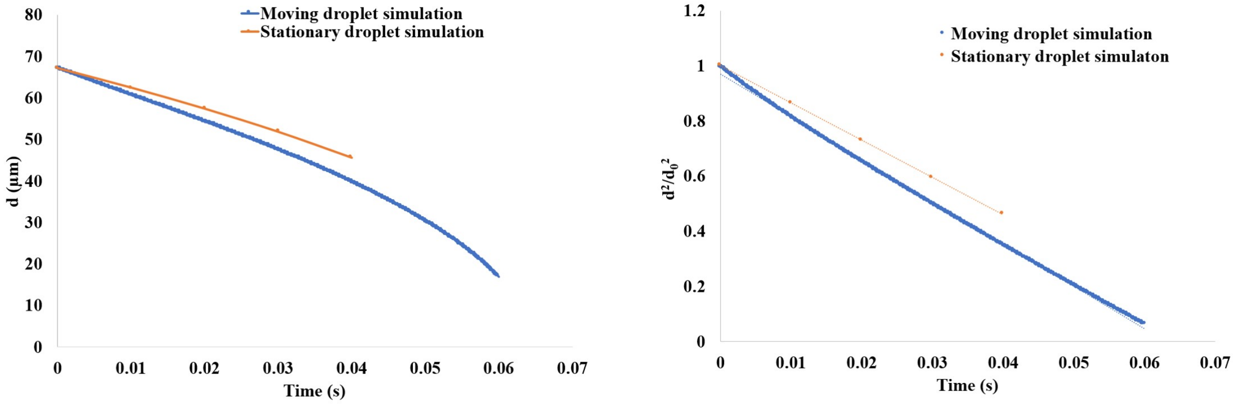

(a) Diameter

(b) Dimensionless diameter

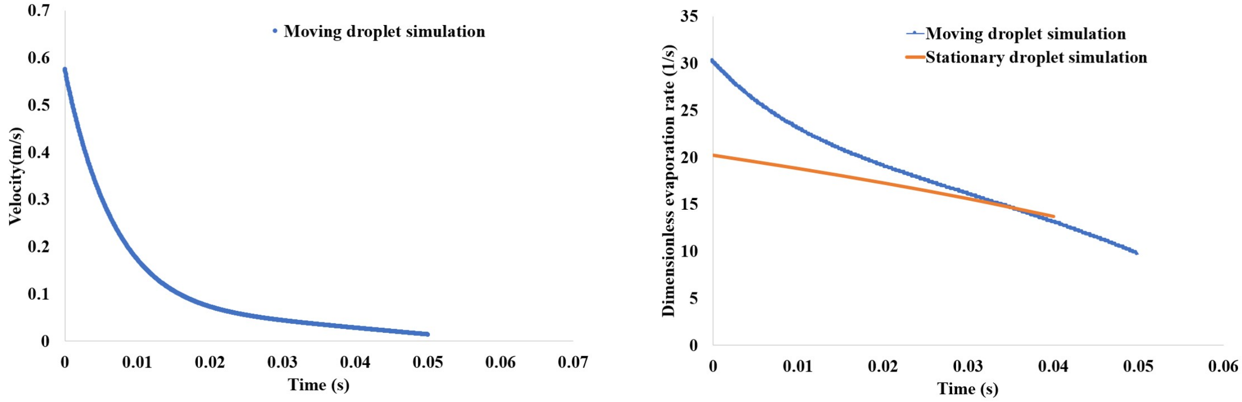

(c) Velocity

(d) Dimensionless evaporation rate

Fig. 3 Simulation of stagnant and moving n-heptane droplet evaporation at 50 °C in the air

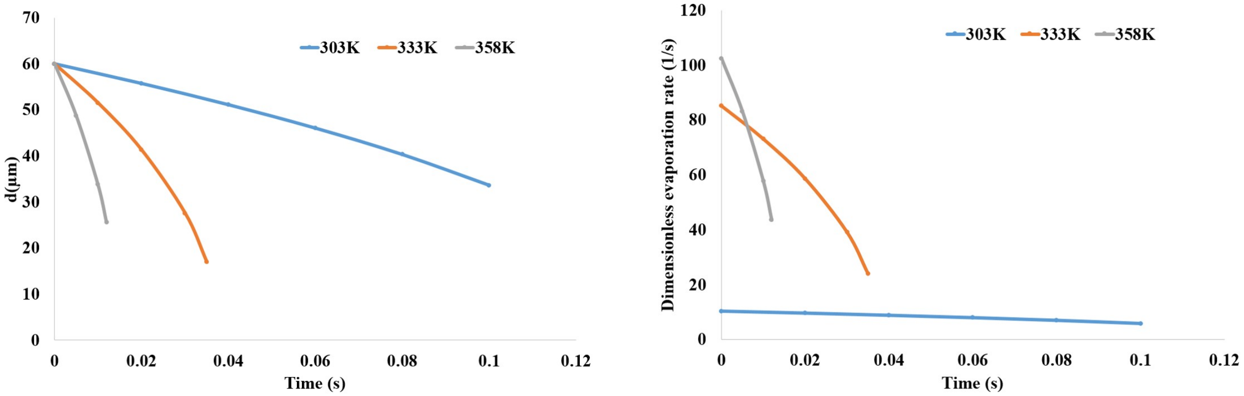

(a) Diameter of stagnant droplet

(b) Evaporation rate of stagnant droplet

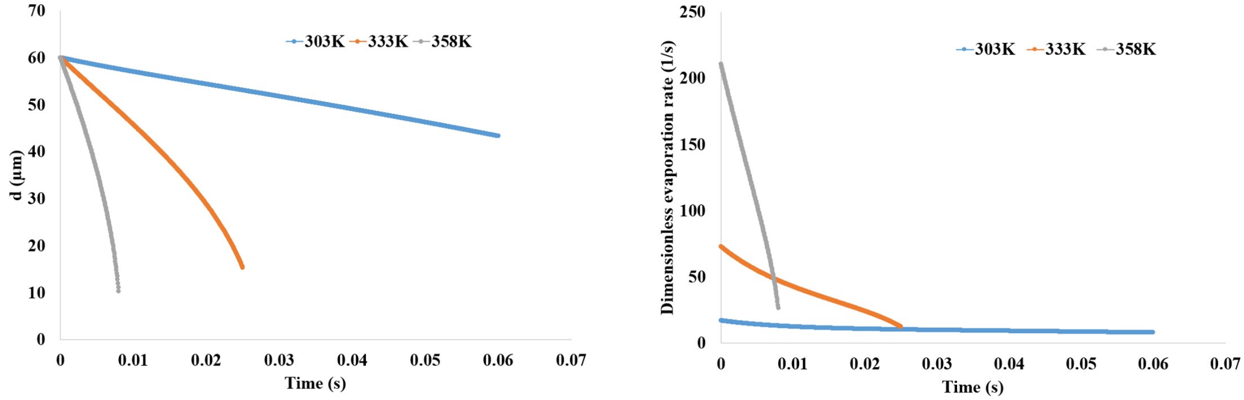

(c) Diameter of moving droplet

(d) Evaporation rate of moving droplet

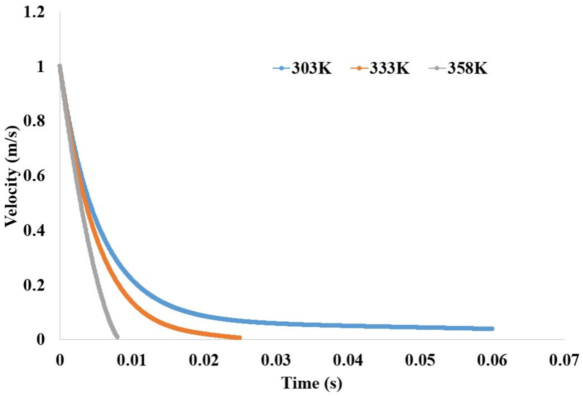

(e) Velocity

Fig. 4 Simulation of stagnant and moving isooctane droplet evaporation in the air at different temperatures

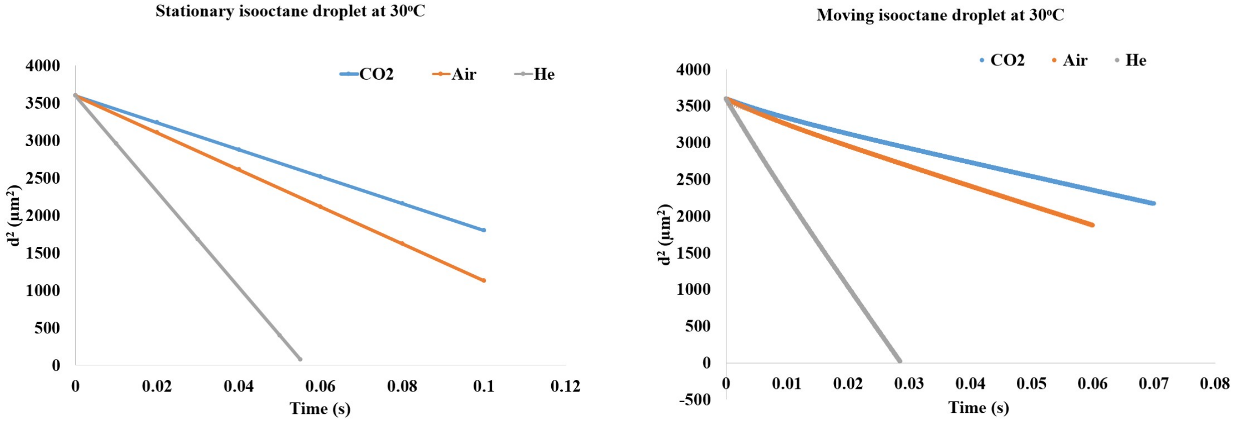

(a) Stagnant droplet

(b) Moving droplet

Fig. 5 Isooctane droplet evaporation at 30 °C in different ambient gases

B. Experimental and simulation results of moving fuel droplet evaporation

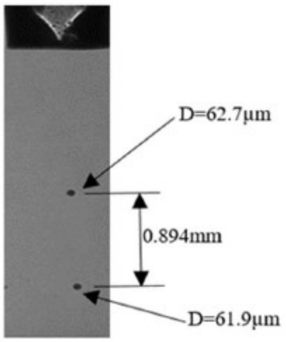

Fig. 6 Camera image showing a trail of n-heptane droplets leaving the nozzle orifice

Figure 6 shows an image of a trail of pure n-heptane droplets after leaving the nozzle. Two adjacent droplets can be seen in the image. The glass nozzle orifice can also be seen in the image, which has a diameter of 30 μm. The two graphs in Figure 7 show a series of results illustrating droplet size change during iso-octane and *n*-heptane droplet evaporation in air at 40 and 50 °C. The initial conditions as extracted from experiments include the initial diameters of the iso-octane droplet with values of 68.7 and 54.3 μm at 40 and 50 °C respectively. The initial velocities corresponding to these two temperatures for iso-octane are 0.812 and 0.563m/s respectively. Initial droplet diameters for n-heptane are 62.7 and 67.2 μm at 40 and 50 °C respectively. The initial velocities corresponding to these two temperatures for n-heptane are 0.626 and 0.576 m/s respectively. The plots of droplet diameter squared show an approximately linear decrease with time. Also, the evaporation at higher temperature leads to faster decrease of droplet diameter and the slope is steeper. There are four data sets in each graph. They correspond to the droplet diameter squared for the experimental and simulation results at two different temperatures. As can be observed, there is a distinct difference in droplet size change as predicted by the simulations and as observed in the experiments. The specific reason for this discrepancy is currently under investigation. The experimental data used in this work is an older data set from a time when the experiment was not set up in an ideal fashion. Issues with humidity control in the chamber, non-constant temperature distribution, misalignment of the LED light source with the camera need to be addressed. These issues have not been resolved currently primarily due to delays resulting from Covid-related shutdown of campus research activities. Further, simulation results could also be the source of error due to assumptions made with respect to uniform temperature distribution in the droplet, or lack of consideration of internal circulation inside the droplet.

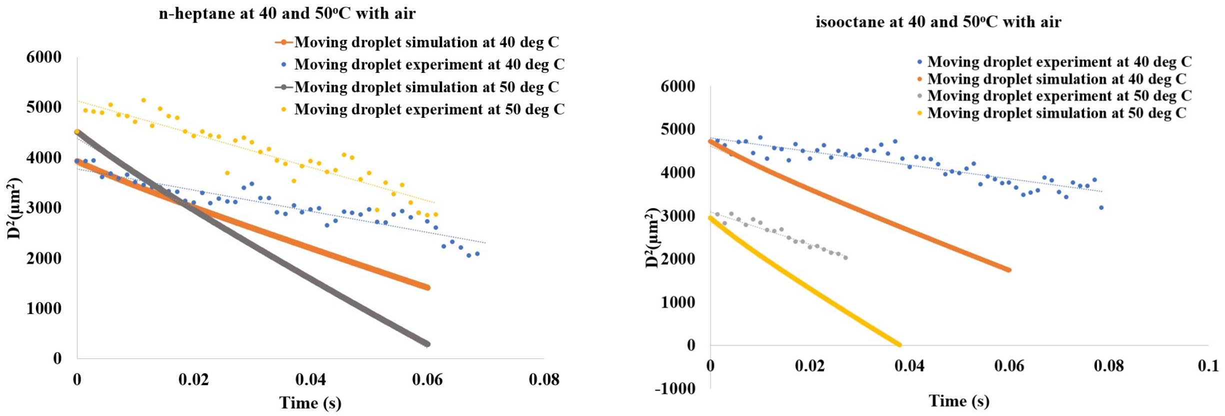

(a) n-heptane

(b) isooctane

Fig. 7 Experimental and simulation results for n-heptane and isooctane droplet evaporation at 40 and 50 °C

C. HOV and vapor pressure prediction for pure fuels

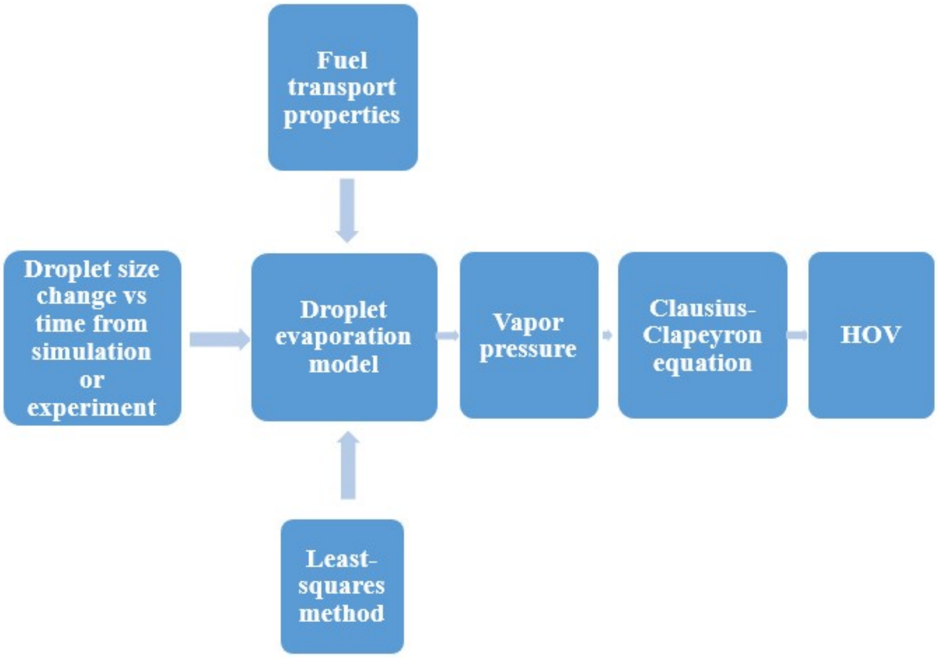

Fig. 8 Flowchart of HOV and vapor pressure prediction

In order to predict HOV and vapor pressure of the pure fuels as a function of temperature, a non-linear least squares approach is used in this work.Using three evaporation slopes for the fuel droplet obtained from simulations of the moving/stationary droplet from three ambient gas compositions as input, the non-linear least squares method applied to Eqn (19) and Eqn (21) is used to give the results for HOV and vapor pressure. The schematic showing the workflow of HOV and vapor pressure prediction is presented in Figure 8. Figures 9, 10, 11 show the results of HOV and vapor pressure for water, iso-octane, and n-heptane at three temperatures using training data obtained from simulations. Results are compared with literature data. Stationary droplet simulation shows the smallest deviation, within 4% for HOV and 9% for vapor pressure. Moving droplet simulation gives a higher deviation of 16% for HOV and 38% for vapor pressure. Figure 12 and 13 present the results for HOV and vapor pressure as obtained from experiments and simulation. The maximum deviations from simulation for HOV is 18% and 27.5% for vapor pressure. The maximum deviations from experiment are 72% for HOV.

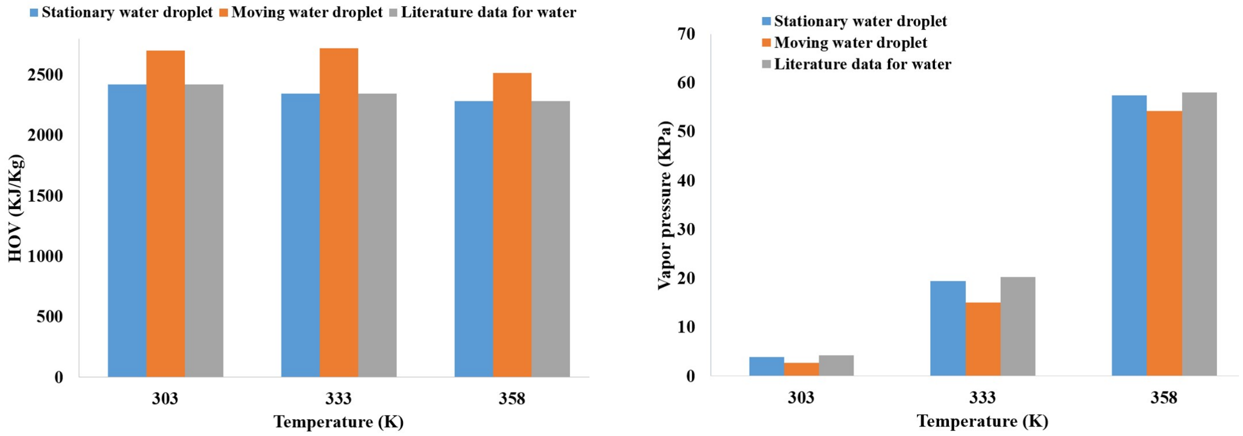

(a) HOV (b) Vapor pressure

Fig. 9 HOV and vapor pressure from water droplet evaporation simulation

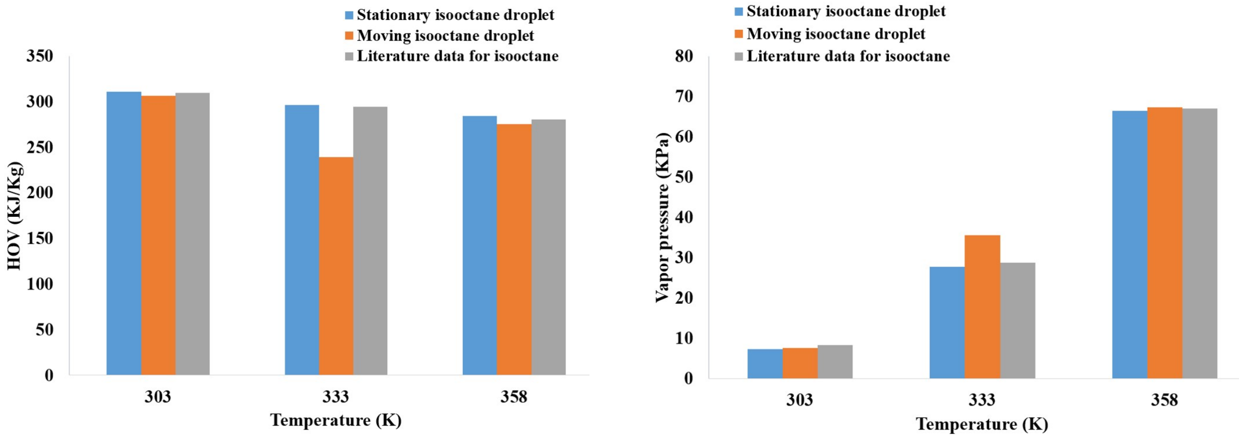

(a) HOV (b) Vapor pressure

Fig. 10 HOV and vapor pressure from isooctane droplet evaporation simulation

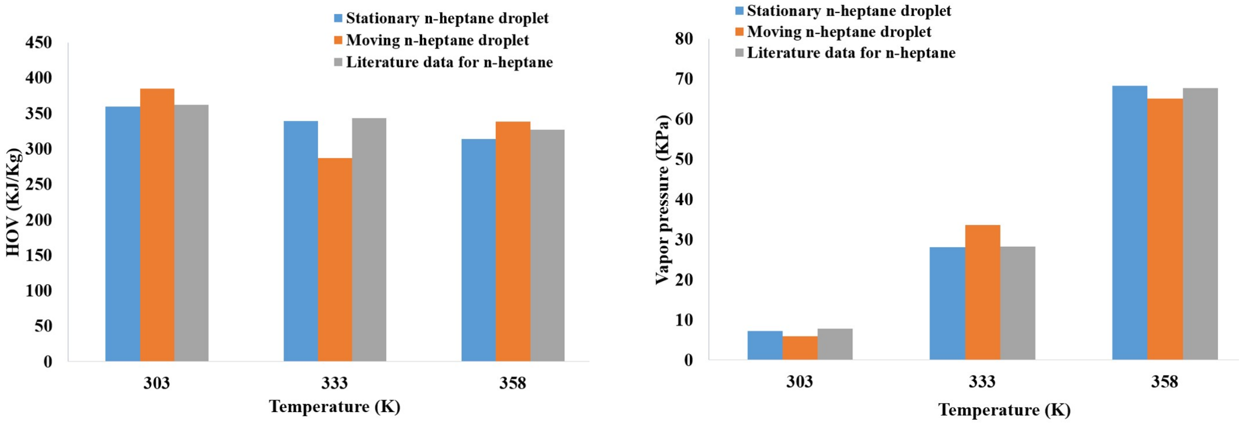

(a) HOV (b) Vapor pressure

Fig. 11 HOV and vapor pressure from n-heptane droplet evaporation simulation

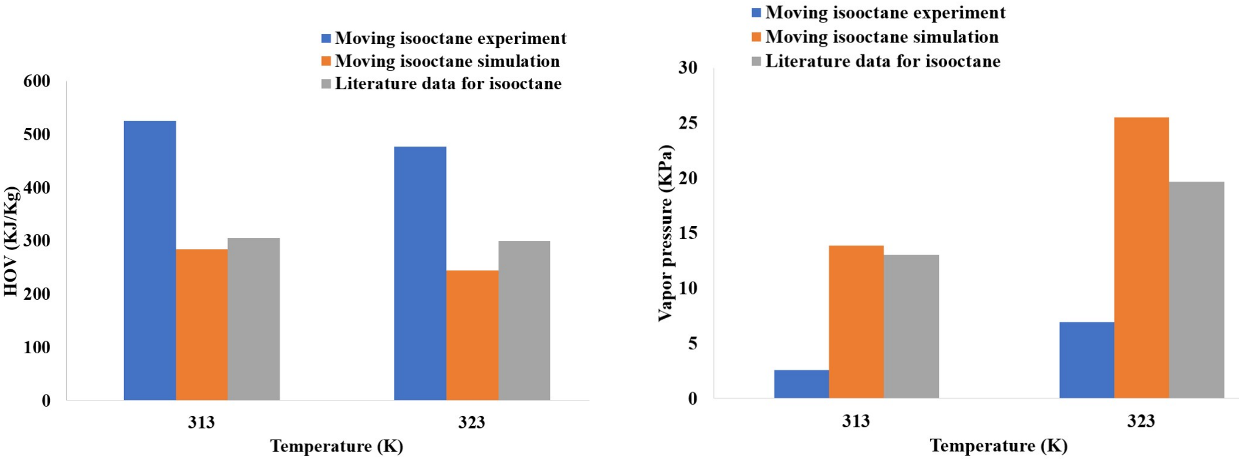

(a) HOV (b) Vapor pressure

Fig. 12 HOV and vapor pressure from isooctane droplet evaporation experiment and simulation at 40 and 50 °C

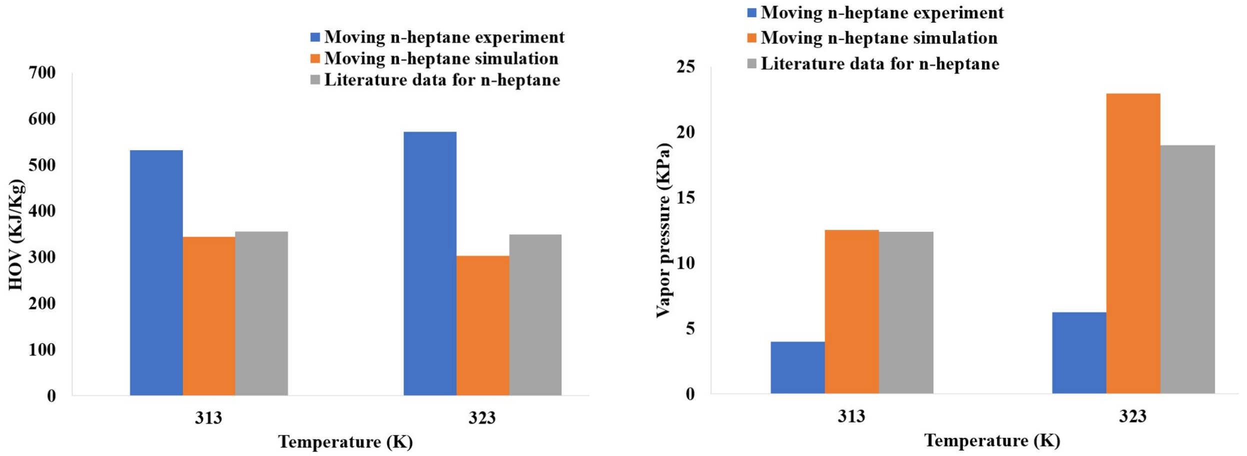

(a) HOV

(b) Vapor pressure

Fig. 13 HOV and vapor pressure from n-heptane droplet evaporation experiment and simulation at 40 and 50 °C

D. HOV prediction for fuel blends

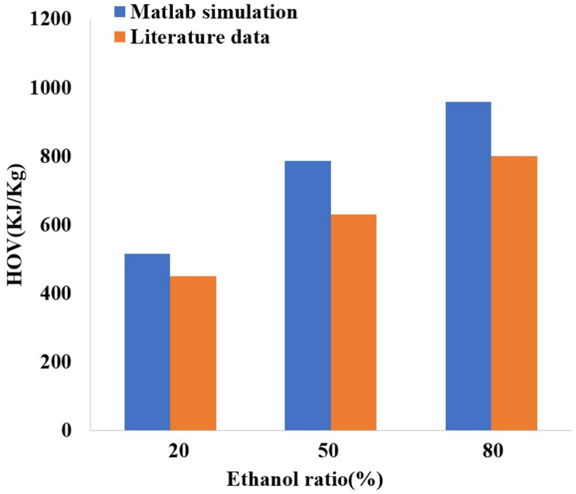

Fig. 14 Heat of vaporization prediction of isooctane and ethanol blends at 25 °C

Besides pure fuel components (iso-octane and n-heptane) considered in this study, there is considerable interest in fuel blends for use in DI gasoline engines. In particular, considerable amount of research has been pursued on ethanol-gasoline blends where bio-derived ethanol can be blended with conventional gasoline fuel. To this end, the simulations for drolet evaporation are carried out for iso-octane/ethanol blends in various volumetric mixing ratios (20-80, 50-50, and 80-20). The simulations are carried out for ambient temperature of 25 °C. Thermophysical properties are evaluated based on the mixing rules for liquid or vapor fuels [16, 17] and are functions of temperature. Reference data for HOV is obtained from Chen and Stone's work [18]. As before, simulations were conducted in three different ambient gas compositions and the non-linear least squares approach was used to estimate HOV and vapor pressure. The deviation between simulation data and reference data is within 25 % as shown in Figure 14.

V. Conclusions and Future Work

This work presents a small-volume, high-throughput approach to measure heat of vaporization and vapor pressure of liquid hydrocarbon fuels for deployment in rapid screening tools. The approach is based on single droplet evaporation of the liquid fuel and use of evaporation slope along with a model for liquid droplet evaporation to estimate vapor pressure. Subsequently the Clausius-Clapeyron equation is used to determine heat of vaporization. The approach is applied to determine heat of vaporization and vapor pressure for water, iso-octane, and n-heptane as a function of temperature. Evaporation slope is calculated from simulations as well as experimental measurements. Simulations include both moving and stationary droplets. The model used for liquid droplet evaporation is the Abramzon-Sirignano model. Results are compared with literature data. The best results are obtained for simulation data corresponding to stagnant droplet evaporation with deviations from reference data being within 4% for HOV and 9% for vapor pressure. Results obtained using moving droplet simulations show higher deviation from literature data up to 16% for HOV and 38% for vapor pressure. Results obtained using experimental data currently show much larger deviation, which is attributed to poor quality of experimental data, and will be revisited in the future. Simulations were also conducted to estimate properties of iso-octane/ethanol blends at 25 °C. Results showed deviation in heat of vaporization to be within 25%.

Future work will include improvements in the experimental setup followed by retaking of experimental data for evaporation of fuel droplets at different temperature conditions. Both pure fuel components as well as blends will be investigated and compared with literature and reference data. Reference data will further be obtained using DSC/TGA tests conducted using standard instruments.

References

[1] Wyszynski, L. P., Stone, C. R., and Kalghatgi, G. T., "The volumetric efficiency of direct and port injection gasoline engines with different fuels," Tech. rep., SAE Technical Paper, 2002.

[2] Ratcliff, M. A., Burton, J., Sindler, P., Christensen, E., Fouts, L., and McCormick, R. L., "Effects of heat of vaporization and octane sensitivity on knock-limited spark ignition engine performance," Tech. rep., SAE Technical Paper, 2018.

[3] Kalghatgi, G., "Fuel anti-knock quality-Part I. Engine studies," *SAE Transactions*, 2001, pp. 1993–2004.

[4] Chupka, G. M., Christensen, E., Fouts, L., Alleman, T. L., Ratcliff, M. A., and McCormick, R. L., "Heat of vaporization measurements for ethanol blends up to 50 volume percent in several hydrocarbon blendstocks and implications for knock in SI engines," *SAE International Journal of Fuels and Lubricants*, Vol. 8, No. 2, 2015, pp. 251–263.

[5] Splitter, D. A., and Szybist, J. P., "Experimental investigation of spark-ignited combustion with high-octane biofuels and EGR. 2. Fuel and EGR effects on knock-limited load and speed," *Energy & Fuels*, Vol. 28, No. 2, 2014, pp. 1432–1445.

[6] Mendes, G., Aleme, H. G., and Barbeira, P. J., "Reid vapor pressure prediction of automotive gasoline using distillation curves and multivariate calibration," *Fuel*, Vol. 187, 2017, pp. 167–172.

[7] Fioroni, G. M., Christensen, E., Fouts, L., and McCormick, R., "Heat of Vaporization and Species Evolution during Gasoline Evaporation Measured by DSC/TGA/MS for Blends of C1 to C4 Alcohols in Commercial Gasoline Blendstocks," Tech. rep., SAE Technical Paper, 2019.

[8] Hatzioannidis, I., Voutsas, E. C., Lois, E., and Tassios, D. P., "Measurement and prediction of Reid vapor pressure of gasoline in the presence of additives," *Journal of Chemical & Engineering Data*, Vol. 43, No. 3, 1998, pp. 386–392.

[9] Kar, K., Last, T., Haywood, C., and Raine, R., "Measurement of Vapor Pressures and Enthalpies of Vaporization of Gasoline and Ethanol Blends and Their Effects on Mixture Preparation in an SI Engine," *SAE Int. J. Fuels Lubr.*, Vol. 1, 2008, pp. 132–144. https://doi.org/10.4271/2008-01-0317, URL https://doi.org/10.4271/2008-01-0317.

[10] McCormick, R. L., Fioroni, G., Fouts, L., Christensen, E., Yanowitz, J., Polikarpov, E., Albrecht, K., Gaspar, D. J., Gladden, J., and George, A., "Selection criteria and screening of potential biomass-derived streams as fuel blendstocks for advanced spark-ignition engines," *SAE International Journal of Fuels and Lubricants*, Vol. 10, No. 2, 2017, pp. 442–460.

[11] Dang, W., Zhao, W., Schoegl, I., and Menon, S., "A small-volume, high-throughput approach for surface tension and viscosity measurements of liquid fuels," *Measurement Science and Technology*, 2020.

[12] Schoegl, I., Sauer, V. M., and Sharma, P., "Predicting combustion characteristics in externally heated micro-tubes," *Combustion and Flame*, Vol. 204, 2019, pp. 33–48.

[13] Peng, . A. S. K., F., “A review of droplet dynamics and vaporization modeling for engineering calculations,” *ASME 1994 International Gas Turbine and Aeroengine Congress and Exposition*, Vol. 3, 1994, pp. Turbo Expo: Power for Land, Sea, and Air.

[14] Abramzon, B., and Sirignano, W., “Droplet vaporization model for spray combustion calculations,” *International journal of heat and mass transfer*, Vol. 32, No. 9, 1989, pp. 1605–1618.

[15] Ray, A. K., Davis, E. J., and Ravindran, P., “Determination of ultra-low vapor pressures by submicron droplet evaporation,” *The Journal of Chemical Physics*, Vol. 71, No. 2, 1979, pp. 582–587. https://doi.org/10.1063/1.438408, URL https://doi.org/10.1063/1.438408.

[16] Goodwin, D. G., Moffat, H. K., and Speth, R. L., “Cantera: An Object-oriented Software Toolkit for Chemical Kinetics, Thermodynamics, and Transport Processes,” http://www.cantera.org, 2017. https://doi.org/10.5281/zenodo.170284, version 2.3.0.

[17] Harstad KG, B. J., “Mixing rules for multicomponent mixture mass diffusion coefficients and thermal diffusion factors,” *The Journal of chemical physics*, Vol. 120, 2004, pp. 5664–73. https://doi.org/10.1063/1.1650296.

[18] Chen, L., and Stone, R., “Measurement of Enthalpies of Vaporization of Isooctane and Ethanol Blends and Their Effects on PM Emissions from a GDI Engine,” *Energy Fuels*, Vol. 25, 2011, pp. 1254–1259.